3 LEED Experiment

This chapter describes specialised equipment and techniques used to perform LEED experiments and to measure intensities of diffracted LEED beams. An overview of the most common setups for experiments will be given. The diffraction geometry is important for the comparison of experimental LEED data with theory and will, thus, be covered in some detail. For the measurement of LEED intensities, close attention will be paid in particular to the preparation of the sample, the accurate alignment of the sample and the physical properties of the detectors, such as the frequently used video cameras. The instrumental response function is one aspect of detectors that can affect the measured intensities, most notably spot profiles used to measure lateral dimensions such as island sizes and disorder. Among various LEED systems that are available on the market, two types will be addressed in relatively more detail, as they provide higher resolution (i.e., are able to detect structural correlations over larger distances along the surface): spot profile analysis LEED (SPA-LEED) and low-energy electron microscope (LEEM). Finally, instrumentation will be described that has been developed for more targeted applications, such as electron-beam sensitive surfaces, and surfaces with micro- or nanoscale structures.

3.1 Experimental Setup

LEED experiments are commonly performed in ultra-high vacuum (UHV) chambers at a base pressure in the range of 10^{-10} mbar or below. Some useful relations between frequently used pressure units are as follows: 1 mbar = 0.75 mmHg, 1 mmHg = 1 Torr, 1 hPa = 1 mbar and 1.333 mbar = 1 Torr. The vacuum conditions are required for two reasons: the electron gun requires a vacuum for its operation and the surface needs a vacuum to remain clean during the measurement. The electron diffraction experiment could be carried out in a vacuum up to about 10^{-6} mbar depending on the composition of the residual gas, but the sample is then usually contaminated or damaged by the ions created by the electron beam passing through the gas, in addition to the adsorption of the residual gas onto the surface. A close packed metal surface with about 3×10^{14} atoms in the surface monolayer would be fully covered within about 1 second at 10^{-6} mbar assuming a sticking coefficient of 1; such a high sticking coefficient applies only to some residual gases (especially oxygen and hydrogen), while most gases would cover the surface or react with it within the required

https://doi.org/10.1017/9781108284578.005 Published online by Cambridge University Press

experimental preparation and measurement times, which can last from many minutes to many hours. The unit 1 Langmuir = 1.33 mbar·sec = 1 torr·sec is used as a convenient unit for gas exposure; see for example [3.1].

Several experimental setups are in use for LEED studies. The most common is the display system to observe the diffraction pattern or to measure the diffraction intensities. LEED is usually applied in the backscattering geometry near normal incidence, and the backscattered diffraction spots are observed. The most frequently used experimental setup is the display system that shows the diffracted spots (corresponding to diffracted beams) either on a fluorescent screen or in a digital image using a 2-D position sensitive detector. The principle of a LEED display system is shown in Figure 3.1.

Both the sample and the first grid are grounded, so the diffracted beams propagate straight through the space between the sample and the first grid. The second and third grids act as a high pass filter to suppress the inelastically scattered electrons. The filter voltage is slightly below the electron energy, typically a few eV, and adjustable. There are three-grid and four-grid systems in use. In the case of a three-grid system there is only one grid at the retarding voltage, giving a slightly worse energy resolution than the four-grid system. The LEED system is also frequently used as a retarding field analyser for Auger electron spectroscopy (AES), and in that case the four-grid version is required. The screen is at high voltage, usually 4–7 keV, to excite the fluorescent screen. The screen is made of glass, and the diffraction spots are observed from the back without disturbance by the grids, although the screen's central portion is then obscured by the electron gun. The system is therefore also called 'reverse view LEED

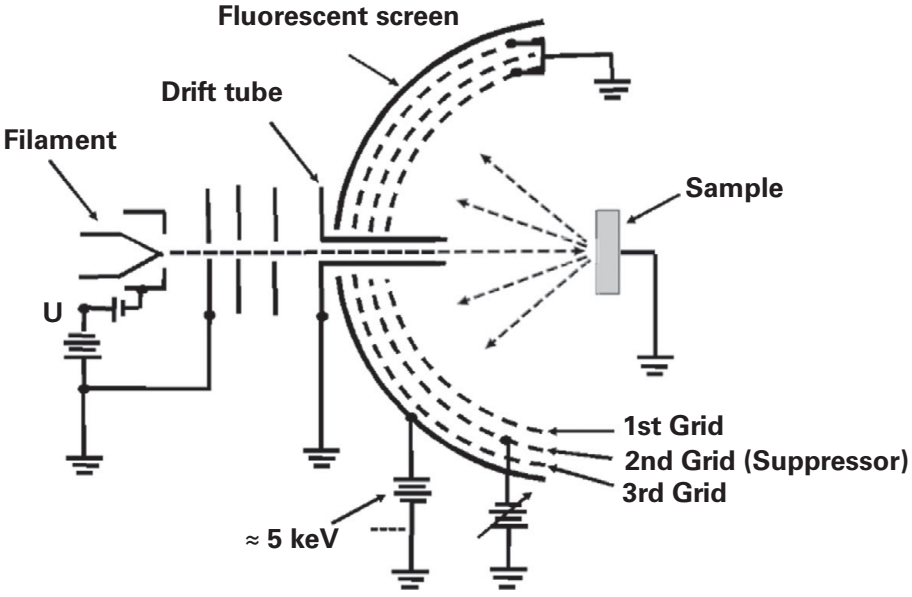

Figure 3.1 Schematic drawing of a three-grid LEED display system using a fluorescent screen. The screen is usually viewed from the left ('rear' or 'back').

https://doi.org/10.1017/9781108284578.005 Published online by Cambridge University Press

optic'. Figure 3.2 shows a schematic of the reverse view arrangement – also called 'back view system' or 'rear view system' – with a spherical glass display screen. Systems with a planar phosphorescent screen are also in use. The spherical screen offers the advantage that the spot pattern has the geometry of the 2D reciprocal lattice of the surface, without distortion when viewed by a distant camera, as illustrated for a square lattice in Figure 3.2(b): the spot pattern shows the same square spot array as the crystal surface. The diffraction intensities are usually recorded by a CCD camera.

The intensity in the diffracted beams can be directly measured with a Faraday cup or a channeltron, also called a channel electron multiplier, and this approach has been used in earlier instruments. More recently, the measurement of intensities has been mostly done with a video camera, as first introduced by P. Heilmann et al. in 1976 [3.3]. Other systems use a 2-D position sensitive detector (microchannel plate) instead of the fluorescent screen, allowing the direct measurement of the intensity and electronic storage of the data.

A different experimental setup is used in high-resolution systems like SPA-LEED (spot profile analysis LEED), with which angular beam profiles are measured [3.4], and low-energy electron microscopy (LEEM), which has a high spatial resolution and allows measurement of LEED intensities from a single structural domain [3.5]. Also, spin-polarised LEED (SPLEED) systems have been developed using a spin-polarised primary beam to allow the measurement of the spin polarisation of the diffracted beams; see for example [3.6] and further references therein.

The diffracted intensities are always recorded on an arbitrary scale but must be normalised to the primary beam intensity, because this incident intensity in most instruments depends on the primary beam's energy. The primary intensity is measured by the current leaving the power supply, not by the sample current, because there are secondary electrons leaving the sample, which affects the net sample current. The current in the diffracted beam is usually on the order of 10^{-2} to 10^{-4} relative to the

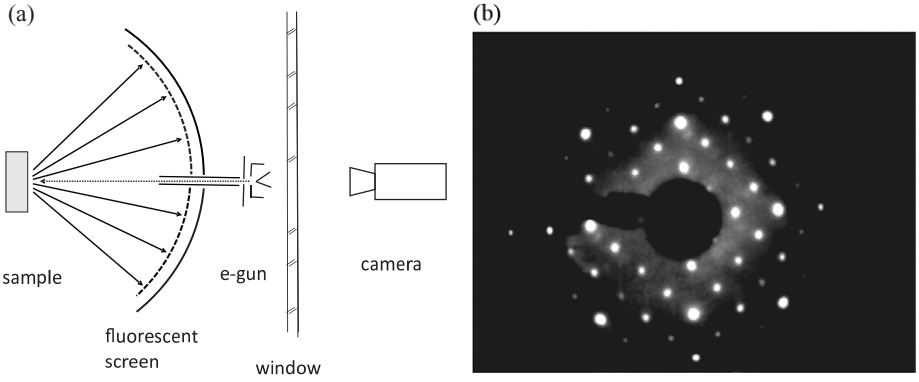

Figure 3.2 (a) Schematic drawing of the experimental 'rear view' LEED setup and the diffraction pattern; (b) Diffraction pattern of $Fe_3O_4(100)$ with a $c(2\times2)$ reconstruction. Reprinted from [3.2]: R. Pentcheva, W. Moritz, J. Rundgren, S. Frank, D. Schrupp and M. Scheffler, *Surf. Sci.*, vol. 602, pp. 1299–1305, 2008, with permission from Elsevier.

https://doi.org/10.1017/9781108284578.005 Published online by Cambridge University Press

primary beam current. Modern video techniques allow the measurement of a complete set of I(V) curves in several minutes.

The distance of the surface plane from the front of the LEED system is usually between 10 and 20 mm, which is not sufficient to install further instruments. Therefore, either the sample or the LEED system must be moved for sample preparation, deposition of adsorbate layers, AES measurements or other analytical investigations. Many commercially available LEED systems therefore offer the possibility to retract the LEED system farther away from the sample. The LEED screen and the grids need to be covered during sample preparation to avoid contamination by sputtering products or material from evaporation sources.

Electrons with the energies applied in LEED are noticeably deflected by the Earth's magnetic field and stray fields from magnetic materials inside the chamber. The Earth's magnetic field therefore must be shielded either by Helmholtz coils, usually mounted outside the UHV chamber, or by a shield of μ-metal, an alloy of high magnetic permeability, placed inside the chamber. The magnetic shielding may not be necessary if only the diffraction pattern will be observed without quantitative interpretation. For I(V) measurements magnetic shielding is required in most cases.

3.2 Diffraction Geometry

The diffraction geometry in reciprocal space is displayed in Figure 3.3. The reciprocal lattice of the 2-D periodic surface is a 2-D lattice of rods oriented perpendicular to the surface plane. The Ewald construction for elastic scattering shows that a reflection occurs whenever the Ewald sphere intersects a lattice rod (see also Section 2.2).

For quantitative structure analysis, one measures the intensity along the lattice rods. This can be done in different ways as shown in Figure 3.4.

The usual approach is to measure the spot intensity with varying energy, producing I(V) curves, where eV is the electron kinetic energy. Changing the angle of incidence or rotating the sample is possible as well but rarely applied, because it induces some uncertainties when the surface is not quite homogeneous, since different patches on the surface may be hit by the primary beam when the sample is rotated. To avoid this source of error requires careful control of the sample position which is rarely reached with the commonly used manipulators. It is sometimes applied, however, to measure data sets at different angles of incidence to extend the amount of data and the reliability of the analysis. It may also be necessary to measure at different incidence angles in cases where only few beams can be measured due to experimental limitations.

At normal incidence the reciprocal lattice of the surface lattice can be directly observed on a display screen. In Figure 3.5(a), a simple hexagonal lattice of atoms is shown. The vectors $\mathbf{a}$, $\mathbf{b}$ mark the (1×1) unit cell, while the vectors $\mathbf{a}'$, $\mathbf{b}'$ are the unit vectors of a $(\sqrt{3}\times\sqrt{3})\mathrm{R}30^\circ$ superlattice, or in matrix notation a $\begin{pmatrix} 2 & 1 \\ -1 & 1 \end{pmatrix}$ superlattice. In Figure 3.5(b), the diffraction pattern and the indices related to the (1×1) unit cell are given; in Figure 3.5(c), the same diffraction pattern with indices related to the

https://doi.org/10.1017/9781108284578.005 Published online by Cambridge University Press

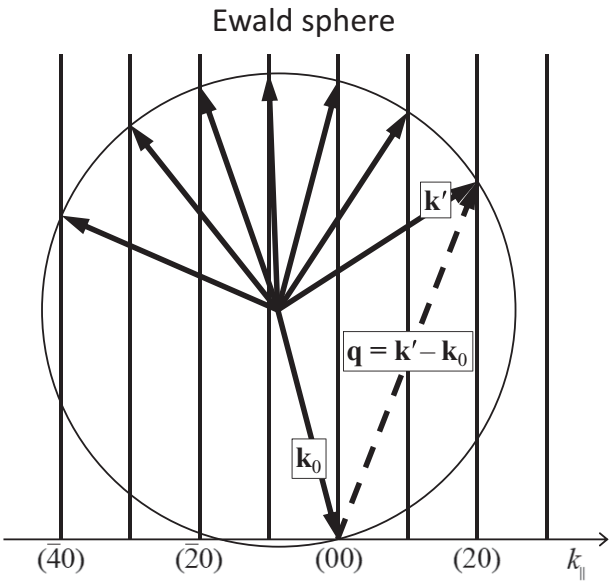

Figure 3.3 Diffraction geometry with Ewald construction of scattering directions of diffracted beams; the surface is horizontal in this representation, with $\mathbf{k}_0$ the incident beam momentum (in the plane of the figure) and $\mathbf{k}'$ one of several possible diffracted beam momenta (the Ewald sphere has radius $|\mathbf{k}_0|$); $\mathbf{q}$ gives the momentum transfer. The vertical lattice rods are given by the reciprocal lattice of the surface lattice.

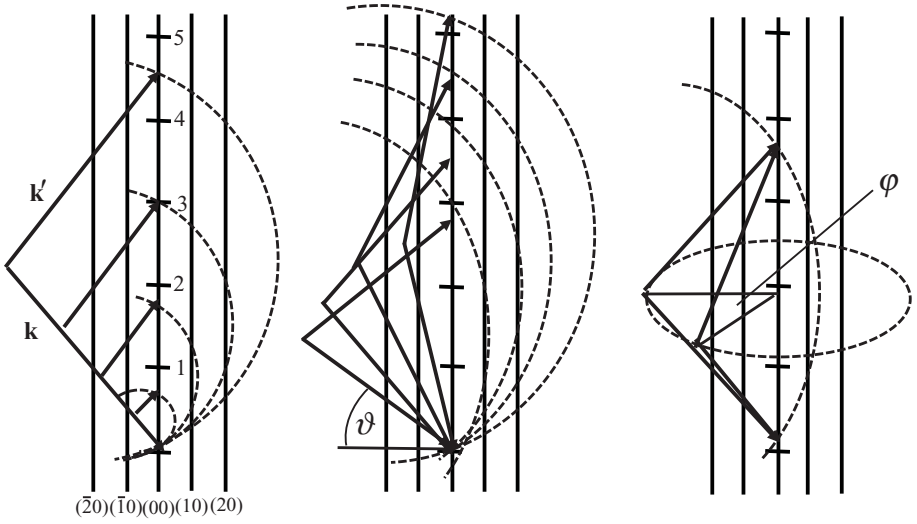

Figure 3.4 Measurement of I(V) curves (left panel), I(ϑ) curves (middle panel) and I(φ) curves (right panel). LEED intensities depend on the polar incidence angle ϑ and on the azimuthal angle φ. The same point in reciprocal space can be reached with different ϑ and change of energy and also with different azimuthal angle φ. In each case different intensities are measured, which is a multiple scattering effect. For kinematical diffraction, the usual case for X-ray diffraction, such dependence would not occur.

https://doi.org/10.1017/9781108284578.005 Published online by Cambridge University Press

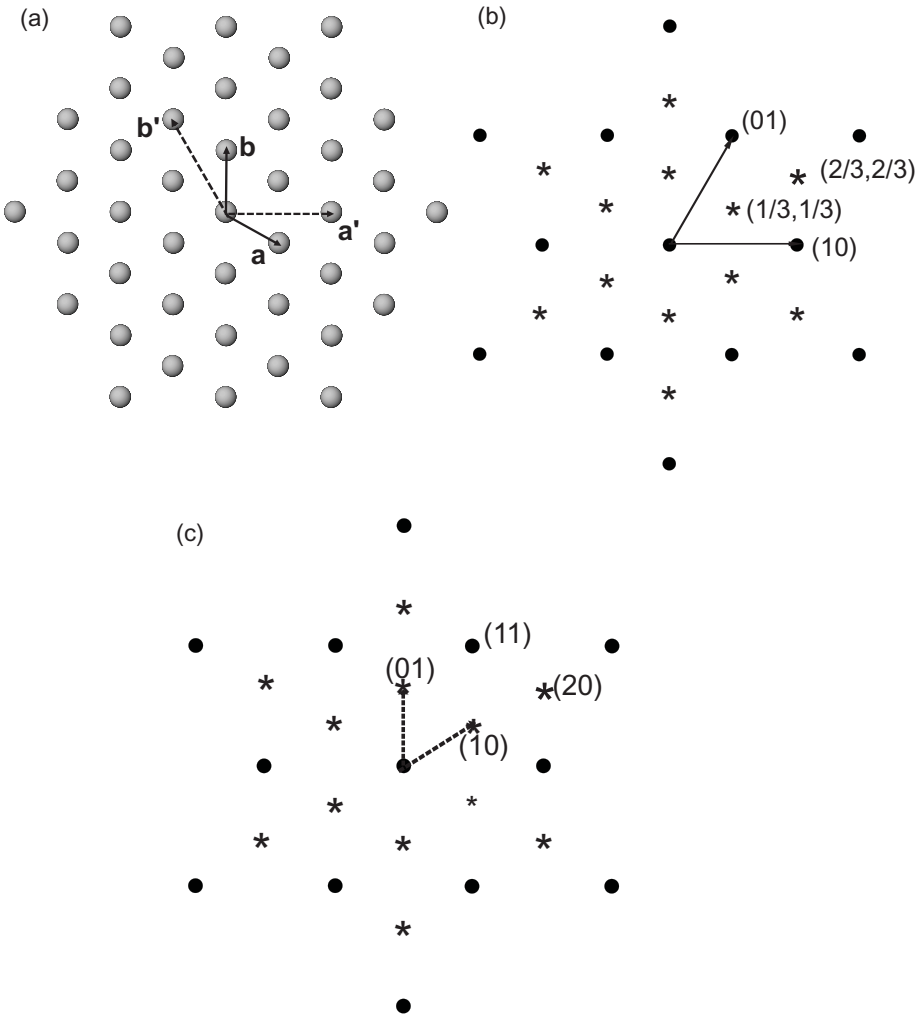

Figure 3.5 (a) Hexagonal lattice and unit cell vectors **a**, **b** for a (1×1) unit cell and **a**′, **b**′ for a $(\sqrt{3}\times\sqrt{3})$R30° superlattice; (b) reciprocal lattice with 'fractional' indices related to the (1×1) unit cell; and (c) with 'integer' indices related to the superlattice.

superlattice cell is shown. The latter is frequently more convenient for superlattices with large unit cells. The transformation matrix for the indices is the same as that for the unit cell vectors; see Section 2.1.10.

The range in reciprocal space accessible to LEED for energies between 50 and 450 eV is displayed in Figure 3.6 for a Ag(111) surface. The positions of the Bragg peaks of the 3-D substrate are indicated in the figure for comparison. It is obvious that the back-scattering geometry used in LEED only allows the measurement of reflections at high momentum transfer normal to the surface corresponding to a high index *l* in the

https://doi.org/10.1017/9781108284578.005 Published online by Cambridge University Press

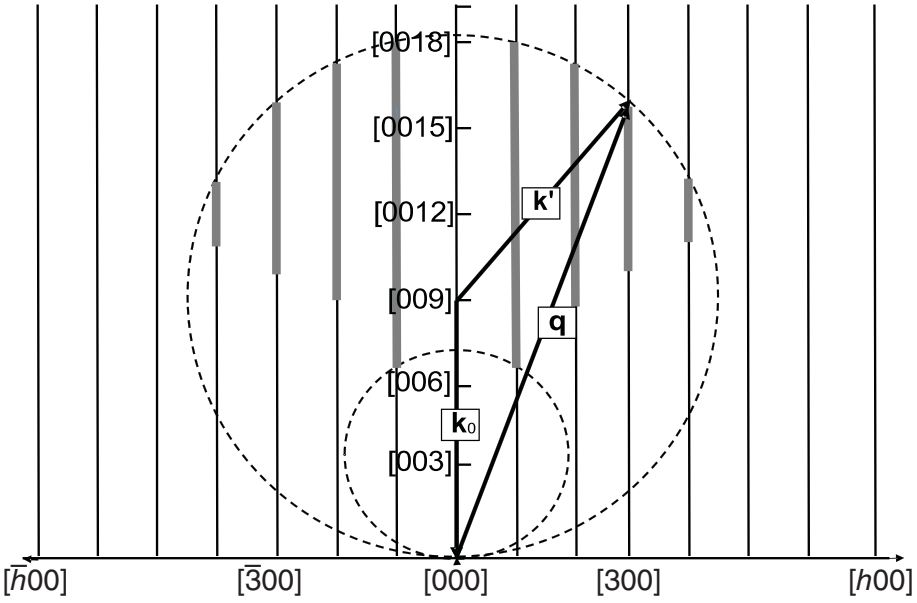

Figure 3.6 Ewald construction for the diffraction angles of the (h0) beams of the Ag(111) surface. The small and large dashed circles correspond to energies of 50 and 450 eV, respectively. The measurable range of the (h0) beams in this energy range is marked in grey on the reciprocal lattice rods. The Bragg points at the (00) beam are marked for reference; $\mathbf{q} = \mathbf{k}' - \mathbf{k}_0$ is the diffraction vector.

reciprocal lattice. LEED intensity analysis is therefore most sensitive to the z-component of the atom positions and less sensitive to the components parallel to the surface. This argument applies to the kinematic or single scattering contribution to the total diffracted intensity, but also partially to the multiple scattering contribution because the scattering amplitude has maxima in the forward and backward directions; see Figure 2.28.

3.3 Measurement of LEED Intensities

There are three basic steps in the measurement of LEED I(V) curves which we shall discuss in the following subsections.

3.3.1 Sample Preparation

While the experimental setup is relatively simple, the experiment itself is more complex to carry out. The quantitative measurement of diffracted intensities requires a planar and homogeneous surface of several square millimeters. An atomically flat and well-ordered surface is required, as reflected in a diffraction pattern with sharp

https://doi.org/10.1017/9781108284578.005 Published online by Cambridge University Press

spots and low background. If the surface is too rough, no diffraction pattern can be observed. It should also be possible to orient the sample to within 0.1°. The manipulator, therefore, should have two independent axes of rotation to align the sample. In many cases the preparation of the sample requires heating it to high temperatures for surface annealing and it is further desirable for intensity measurements to cool the crystal to liquid nitrogen or lower temperatures. To investigate insulating surfaces (which charge up under an incident LEED beam and thereby prevent or complicate diffraction), one may grow a thin insulating film on metal or semiconductor surfaces such that the conductivity is large enough to prevent the probe from charging.

Different methods are used to prepare clean surfaces in UHV depending on the material. The meaning of 'clean' must be defined first as it depends on the planned experiments and the experimental methods used to control the contamination. For LEED measurements on metal surfaces and adsorbate layers on metal surfaces, frequently AES is used to check that the surface is substantially free of contaminants after each preparation (except for H, which is not detectable by AES). It is also necessary to check that the surface is still not contaminated after measurement. The detection limit of AES is usually in the range of 10^{-3} monolayers. This is sufficient for LEED I(V) measurements but may not be sufficient for the preparation of well-ordered adsorbate layers. It should also be kept in mind that a sharp LEED pattern with low background does not guarantee a contamination-free surface. LEED from ordered surfaces is not very sensitive to a low concentration of defects. Therefore, the cleanliness is often controlled by scanning tunnelling microscopy (STM), with which technique single contaminant atoms may become visible. The disadvantage is that the area investigated by STM is usually much smaller than the area covered by the LEED beam. The cleanliness of a surface can also be very sensitively controlled by photoemission if this technique is available.

Different methods exist to prepare clean and well-ordered surfaces in UHV. Some materials, such as alkali halides, can be cleaved in UHV, while others can be cleaned by chemical reaction and desorption (e.g., oxidising C contaminants on the surface and subsequent desorption of CO is used to remove C from several metal surfaces or removing O on the surface by reaction with H_2 and subsequent desorption of H_2O). The main method used for preparing clean metal surfaces is ion bombardment (sputtering) and annealing. For ion bombardment, usually Ar^+ ions are used in the energy range between 500 and 1500 eV, because in this energy range the impact on the surface atoms is large enough to remove them from the surface. At higher energies the probability increases that Ar^+ ions penetrate into deeper layers and get stuck there. It depends on the material whether Ar can be removed from the surface region by annealing or not. This annealing often also brings other near-surface bulk impurities to the surface, requiring further cycles of ion bombardment and annealing and helping reduce later surface segregation of bulk impurities. With surfaces of bulk compounds, such as alloys and oxides, the aforementioned surface preparation methods can also produce non-bulk-like

https://doi.org/10.1017/9781108284578.005 Published online by Cambridge University Press

segregation and ordering of the bulk components near the surface, thereby altering its composition and structure.

More detailed discussions of ion bombardment are given by L. S. Dake et al. [3.7] and by H. Ibach [3.1] where the preparation of semiconductor surfaces is also summarised. A description of preparation methods of metal surfaces can be found in the overview given by C. Becker [3.8] and for transition metal compounds by C. Crotti et al. [3.9]. The preparation on thin oxide films has been described by M. Sterrer and H.-J. Freund [3.10].

3.3.2 Accurate Alignment

Normal incidence is preferred whenever the surface exhibits a rotational symmetry; when only a mirror plane or glide plane exists the incident beam should be in this plane. The proof of whether these conditions are fulfilled is made by comparing the intensities of beams that should be symmetrically equivalent. Control is usually achieved by comparing symmetrically equivalent beams at normal incidence. The general strategy is to adjust the sample orientation at first by comparing symmetrically equivalent I(V) curves at high energies (above 200 eV). The adjustment is made mechanically by means of the manipulator. It is required that the manipulator allow adjustment in two independent rotations. In a second step this position is kept and the adjustment at low energies is done by adjusting the magnetic field compensation. These steps should be repeated until finally the symmetrically equivalent I(V) curves agree in the complete energy range.

The incidence angle should be controlled with an accuracy of $<0.1°$. In Figure 3.7 the I(V) curves of five among six symmetrically equivalent beams of $Fe_2O_3(0001)$ are shown (the sixth was shadowed by the gun) [3.11]. The incident beam is aligned to the lattice plane, not to the surface normal. A slight miscut away from the lattice plane orientation does not produce significantly different intensities unless it becomes

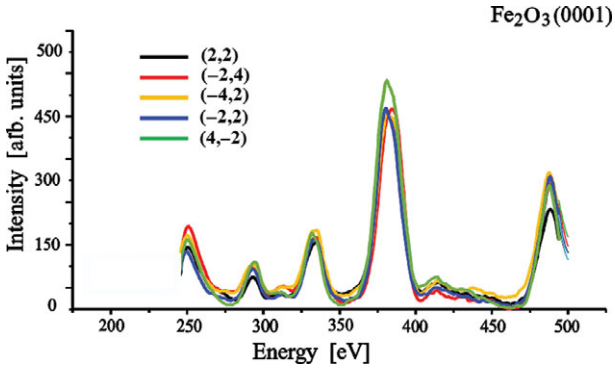

Figure 3.7 Intensities from five of six supposedly symmetrically equivalent beams near normal incidence from $Fe_2O_3(0001)$

https://doi.org/10.1017/9781108284578.005 Published online by Cambridge University Press

visible by beam splitting or by an elliptical shape of the reflections. The differences in the peak maxima may be caused by remaining misalignment or inhomogeneities of the screen. These differences are tolerable: decisive are the matching peak energies, since these most directly affect atomic coordinates. The symmetrically equivalent beams are averaged together to further reduce errors and the averaged curve is used for the subsequent structural analysis.

It should be noted that the comparison of one beam between experiment and theory is not sufficient, as discussed in Section 6.1.2: the peak positions should match for all beams. In general, the I(V) curves of all beams visible on the screen should be measured. The average of symmetrically equivalent beams and the mean square deviation is then stored in a separate file to be used for the analysis. The mean square deviation can be used for the calculation of error estimates as discussed in Section 6.1.3.

There are cases where it is not possible to align the sample precisely (e.g., when the manipulator is not equipped with rotation axes or when the sample does not possess a symmetry which could be used for alignment). For example, in the case of stepped surfaces a mirror plane can often be used to align the incident beam in the mirror plane. This fixes the azimuthal angle φ of the incident beam while the polar angle ϑ (see Figure 3.8(a)) remains to be determined. It may not be possible to determine the polar angle precisely enough from the diffraction pattern: then the polar angle must be determined in the analysis by taking it as an additional parameter to be optimised.

In cases where the beams can be indexed and the lattice constants of the substrate are known, the incidence angle can be determined from the position of the beams on the screen. The method has been described previously by S. L. Cunningham and W. H. Weinberg [3.12] and by M. A. Van Hove et al. [3.13], and will only be summarised here.

The incident wave vector in the laboratory frame is $\mathbf{k}_l^i$ and in the crystal frame $\mathbf{k}_c^i$. The incident wave in the laboratory frame has only a z_l component and is given by

$$k_{lz}^i = k = \frac{\sqrt{2m_e E}}{\hbar}, \tag{3.1}$$

where E is the electron energy relative to vacuum zero, m_e is the free electron mass and $\hbar$ is Planck's constant. The transformation matrix which relates a vector $\mathbf{k}_c^i$ in the crystal frame to a vector $\mathbf{k}_l^i$ in the laboratory frame is given by

$$\mathbf{k}_c^i = \begin{pmatrix} -\sin\varphi & -\cos\vartheta\cos\varphi & \sin\vartheta\cos\varphi \\ \cos\varphi & -\cos\vartheta\sin\varphi & \sin\vartheta\sin\varphi \\ 0 & \sin\vartheta & \cos\vartheta \end{pmatrix} \mathbf{k}_l^i, \tag{3.2}$$

where $\varphi = -\psi - \pi/2$. In the crystal frame, the incident wave vector is given by

$$\begin{aligned} k_{cx}^i &= k\sin\vartheta\cos\varphi, \\ k_{cy}^i &= k\sin\vartheta\sin\varphi, \\ k_{cz}^i &= k\cos\vartheta. \end{aligned} \tag{3.3}$$

https://doi.org/10.1017/9781108284578.005 Published online by Cambridge University Press

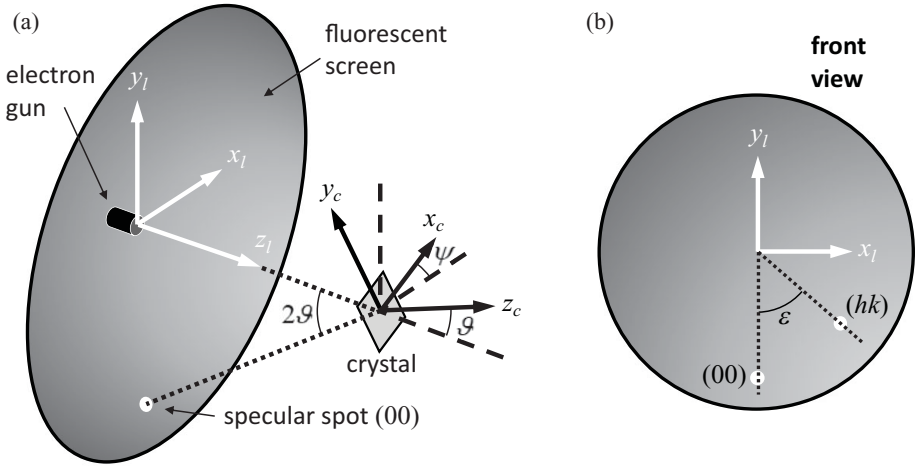

Figure 3.8 (a) Schematic of the LEED experiment showing the laboratory coordinate system (x_l, y_l, z_l), as related to the hemispherical fluorescent screen and electron gun, and the crystal coordinate system (x_c, y_c, z_c). The two systems are related by the angles ϑ and $\psi = -\varphi - \pi/2$. (b) Front view of the fluorescent screen showing the definitions of the laboratory y-axis and the angle ε for the (hk) LEED spot.

Upon scattering from the crystal, the (hk) diffracted beam has the wave vector components

$$\begin{aligned} k^s_{cx} &= k^i_{cx} + g_x(hk), \\ k^s_{cy} &= k^i_{cy} + g_y(hk), \\ k^s_{cz} &= -\sqrt{k^2 - \left(k^s_{cx}\right)^2 - \left(k^s_{cy}\right)^2}. \end{aligned} \tag{3.4}$$

Here, $\mathbf{g}(hk)$ is the (hk) reciprocal lattice vector, and the z_c-component is determined by energy conservation. Finally, using the transpose of Eq. (3.2), the scattered wave components in the laboratory frame are given by

$$\begin{aligned} k^s_{lx} &= -k^s_{cx}\sin\varphi + k^s_{cy}\cos\varphi, \\ k^s_{ly} &= -k^s_{cx}\cos\vartheta\cos\varphi - k^s_{cy}\cos\vartheta\sin\varphi + k^s_{cz}\sin\vartheta. \end{aligned} \tag{3.5}$$

From a LEED photograph, the angle $\varepsilon(hk)$ between the y_l axis and the (hk) spot (see Figure 3.8(b)) is related to the wave vector components by

$$\tan\varepsilon(hk) = \frac{k^s_{lx}}{-k^s_{ly}}. \tag{3.6}$$

For a single spot, Eq. (3.6) is a single equation with two unknowns. Therefore, in principle, any two spots on the photograph [other than the (00) spot which defines the y_l axis] can be used to determine the angles ϑ and φ. For any two chosen spots,

https://doi.org/10.1017/9781108284578.005 Published online by Cambridge University Press

labelled $n = 1$ and 2, Eq. (3.6) represents two highly non-linear equations in two unknowns. These may be solved numerically by using Newton's method. The equations can be written as:

$$f_n(\vartheta, \varphi) = k_{lx}^s + k_{ly}^s \tan \varepsilon(hk) = 0, \ \ n = 1, 2. \tag{3.7}$$

For the i-th iteration, the (2×2) matrix equation

$$\begin{pmatrix} J_{1\vartheta} & J_{1\varphi} \\ J_{2\vartheta} & J_{2\varphi} \end{pmatrix} \begin{pmatrix} \Delta\vartheta \\ \Delta\varphi \end{pmatrix} = \begin{pmatrix} -f_1(\vartheta_i, \varphi_i) \\ -f_2(\vartheta_i, \varphi_i) \end{pmatrix} \tag{3.8}$$

is solved numerically for $\Delta\vartheta$ and $\Delta\varphi$, where J is the Jacobian matrix given by, for example,

$$J_{1\vartheta} = \left. \frac{\partial f_1(\vartheta, \varphi)}{\partial \vartheta} \right|_{\vartheta_i, \varphi_i}, \text{etc.} \tag{3.9}$$

New values of ϑ and φ are determined by

$$\begin{aligned} \vartheta_{i+1} &= \vartheta_i + \Delta\vartheta \\ \varphi_{i+1} &= \varphi_i + \Delta\varphi, \end{aligned} \tag{3.10}$$

and the procedure is repeated until $\Delta\vartheta$ and $\Delta\varphi$ are less than, for example, 10^{-3} rad. This numerical procedure is quite rapid due partly to the fact that the Jacobian is analytic. One advantage of this technique is that the angle $\varepsilon(hk)$ does not depend on the location of the crystal: the angle $\varepsilon(hk)$ is invariant as the crystal is moved along the axis of the hemispherical screen (assuming that the electron beam is collinear with this axis). It is important, however, that the camera also be located on this axis, so care must be taken in this alignment. An example for the determination of the incidence angle at Ir(111) is given in [3.12].

This method of determining the angles of incidence in a LEED experiment is both accurate and simple. The method is accurate because the angles are determined many times from a single photograph. Absolute accuracies of less than 0.1° should be attainable routinely. The method is simple in that it requires only a camera. In addition, there is no need for a calibration point (such as normal incidence) to be established. However, it should be noted that the above procedure is applicable only when the electron gun is collinear with the axis of the camera. A related method was developed by G. P. Price [3.14] to determine the incident and azimuthal angles by treating the position of the electron gun and the electron energy as unknowns and using at least three LEED spots, including the specular (00) beam. This method, however, requires the crystal to be positioned precisely at the centre of curvature of the LEED screen. In addition, both methods require that the incident electron beam be aligned with the centre of curvature of the LEED screen. Under special circumstances when the crystal is off-centre or the electron gun is misaligned, a more general method developed by A. C. Sobrero and W. H. Weinberg [3.15] should be used. This method can be used to check the alignment of the electron gun and the position of the crystal, in addition to determining the polar and azimuthal angles of incidence.

https://doi.org/10.1017/9781108284578.005 Published online by Cambridge University Press

A similar method, also based on the knowledge of the beam indices, has been described by F. Sojka et al. [3.16; 3.17] to correct deviations from normal incidence for the precise determination of lattice constants with high-resolution LEED systems.

Further methods have been developed to determine the angles of incidence which are especially useful for studies with SPA-LEED when a second external electron gun and a large angle of incidence are used [3.18]. Such an arrangement allows the observation of morphological changes during homo- or hetero-epitaxial growth and the measurement of the strain state at different coverages. The precise knowledge of the incidence angle is essential in such studies. The authors describe four different cases where the polar angle ϑ of the incident beam can be determined. The first method is based on the fact that in the reciprocal net a constant distance exists between beams of a Laue zone while the incidence angle can be derived from the measurable distance on the screen (see Figure 3.9).

This method has the advantage that no knowledge about the lattice constants nor about the beam indices is required.

The second and third case apply to growth experiments and rough surfaces. The method utilises the fact that steps on surfaces cause an oscillation of the beam width and of the peak intensity of the (00) beam with energy. This effect is used to observe layer-by-layer growth in epitaxial growth but occurs on every surface with a non-zero step density. It is required that the interlayer distance be known. Maxima of the peak

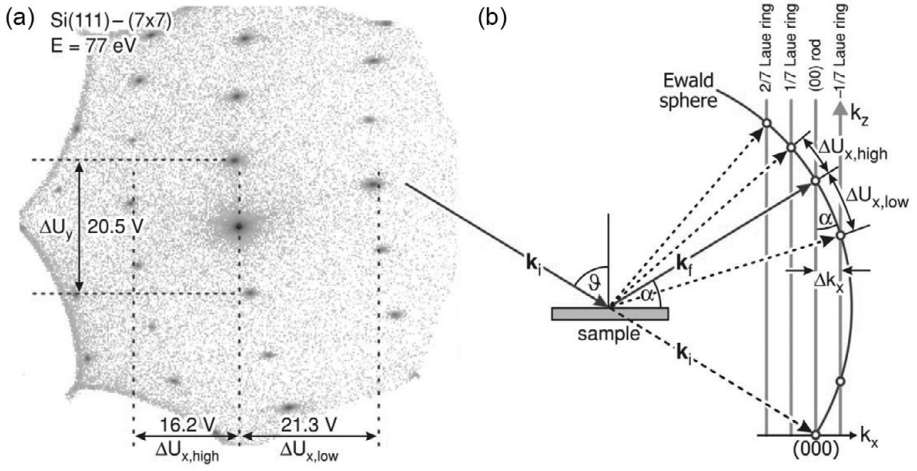

Figure 3.9 (a) LEED pattern for Si(111)–(7×7), recorded with the external electron gun at 77 eV. The intensity is displayed on an inverse logarithmic scale. The distances $\Delta U_{x,\mathrm{low}}$, $\Delta U_{x,\mathrm{high}}$ and ΔU_y between the Laue rings and the first 1/7 peaks are indicated. (b) Ewald construction for large angles of incidence for an external electron gun geometry. The scan is located on the Ewald sphere, where the y direction of the LEED picture is perpendicular to k_z and k_x. Reprinted from [3.18] C. Klein, T. Nabbefeld, H. Hattab, D. Meyer, G. Jnawali, M. Kammler, F.-J. Meyer zu Heringdorf, A. Golla-Franz, B. H. Müller, Th. Schmidt, M. Henzler and M. Horn-von Hoegen, *Rev. Sci. Instrum.*, vol. 82, p. 035111, 2011, with the permission of AIP Publishing.

https://doi.org/10.1017/9781108284578.005 Published online by Cambridge University Press

intensity occur at the Bragg points, while minima occur between the Bragg points. The position of the maxima and minima on the energy scale depends on the normal component S of the momentum transfer:

$$S = 2d\left(k'_z - k^0_z\right) = 2d|\mathbf{k}|\cos\vartheta \tag{3.11}$$

where d is the normal distance between layers and $S = n2\pi$. At integer values of n, the peak intensity of the (00) beam has maxima, as illustrated in Figure 3.10. The angle of incidence ϑ can be derived from the fit of the energy dependence on the peak intensity. This is, by the way, not influenced by the inner potential by which the energy of the electron beam inside the crystal is increased, since the interference between the diffracted beams from different terraces occurs outside the crystal [3.19]. The fourth case applies to faceting of the surface after deposition of an adsorbate. From the

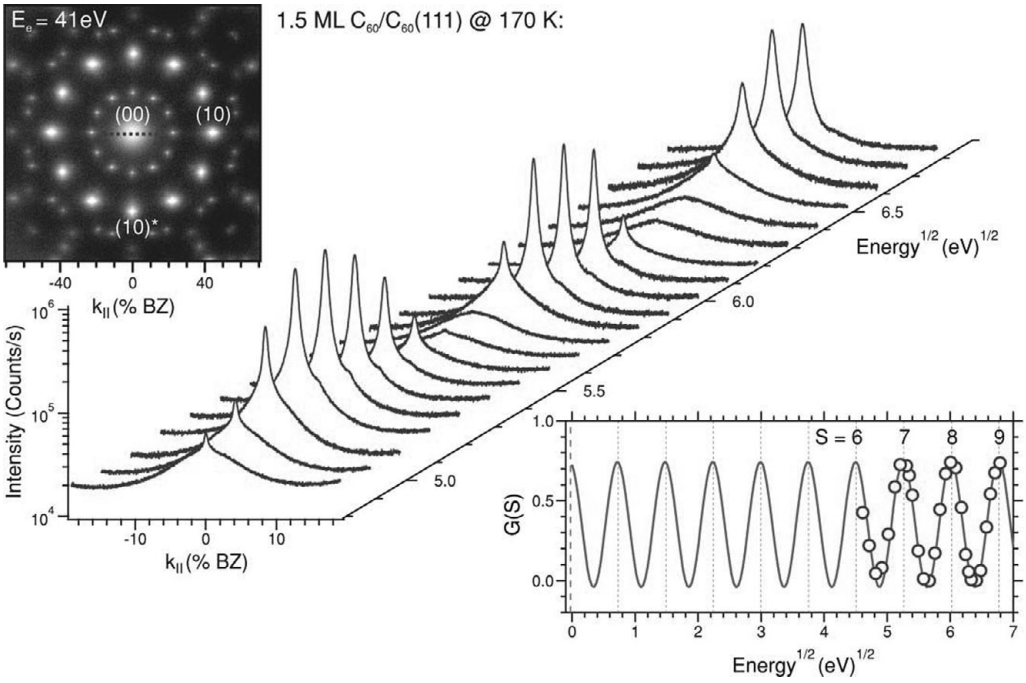

Figure 3.10 Upper left: LEED pattern of a rough C_{60}(111) surface at 41 eV. Centre: (00) spot profiles as a function of the electron energy. The periodic variation between sharp spots at the 'in-phase' or Bragg condition and broad spots at the 'out-of-phase' or anti-Bragg condition is clearly visible. Bottom right: The ratio of the central spike intensity to the total intensity $G(S)$ is plotted as a function of the square root of the electron energy. The order of the Bragg conditions (integer scattering phase S) is determined from the oscillation period and the boundary condition at zero energy. Reprinted from [3.18] C. Klein, T. Nabbefeld, H. Hattab, D. Meyer, G. Jnawali, M. Kammler, F.-J. Meyer zu Heringdorf, A. Golla-Franz, B. H. Müller, Th. Schmidt, M. Henzler and M. Horn-von Hoegen, *Rev. Sci. Instrum.*, vol. 82, p. 035111, 2011, with the permission of AIP Publishing.

https://doi.org/10.1017/9781108284578.005 Published online by Cambridge University Press

intersection of the (00) rods of two facets the orientation of the facet and the angle of incidence can be derived.

3.3.3 Measurement of LEED Intensities with a Video System

With a rear-view LEED system and a fluorescent screen, the diffracted intensities are frequently measured by using a video system. The resulting beam intensities are typically reported on an arbitrary scale but must be normalised to the intensity of the primary beam. The manufacturer usually provides a program to measure I(V) curves of selected beams. There is also similar software available from independent companies. The intensity is integrated over an area around the centre of the spot and the background is subtracted; this background is taken as the average intensity on the rim of an area surrounding the peaks, scaled by the area of the peak. The area of the peak can be set in the program. An improved procedure for the extraction of diffraction intensities from LEED images uses a 2-D fit of the peak with a Gaussian profile and interpolation of the background; see Figure 3.11, as described by K. M. Schindler et al. [3.20]. The improvements in the removal of background intensity and the tracking of spot positions are shown in Figure 3.12 together with the I(V) curve obtained by a simple background subtraction. The precision and accuracy of the LEED I(V) analysis are substantially increased using this evaluation of LEED images.

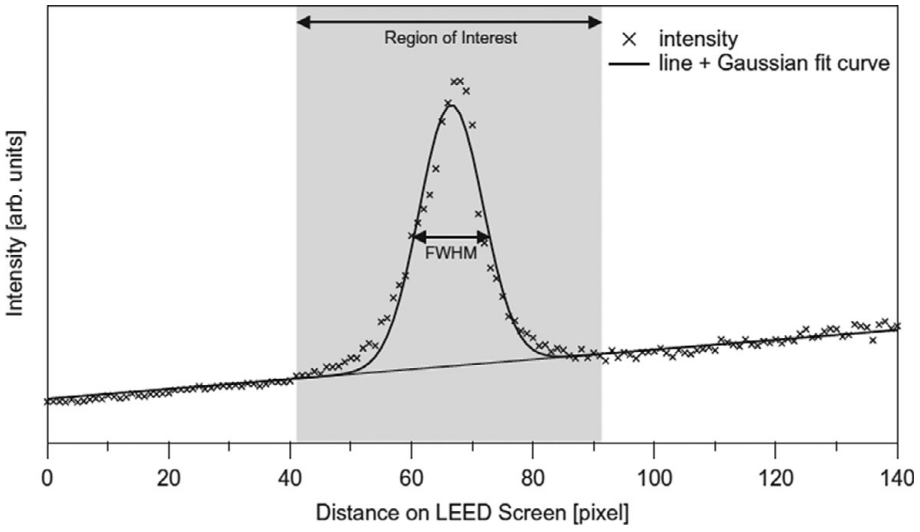

Figure 3.11 Line profile through a diffraction spot, with the fit curve (Gaussian on a line) and the derived region of interest (shaded band); the abscissa, representing angle of diffraction, has arbitrary units. Reprinted from [3.20] K. M. Schindler, M. Huth and W. Widdra, *Chem. Phys. Lett.*, vol. 532, pp. 116–118, 2012, with permission from Elsevier.

https://doi.org/10.1017/9781108284578.005 Published online by Cambridge University Press

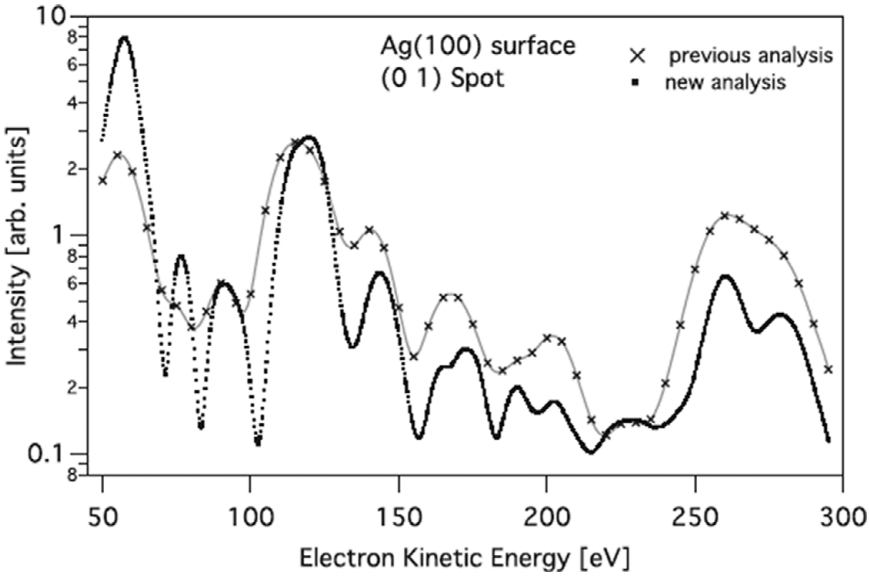

Figure 3.12 Experimental LEED I(V) curves of the clean Ag(001) surface for the (01) diffraction spot. Line marked with ×: simple background subtraction. Dotted line: fit background and subtraction showing a better resolution and a larger dynamic range. The new analysis has been performed with an improved integration of the spot intensity and subtraction of the background. Reprinted from [3.20] K. M. Schindler, M. Huth and W. Widdra, *Chem. Phys. Lett.*, vol. 532, pp. 116–118, 2012, with permission from Elsevier.

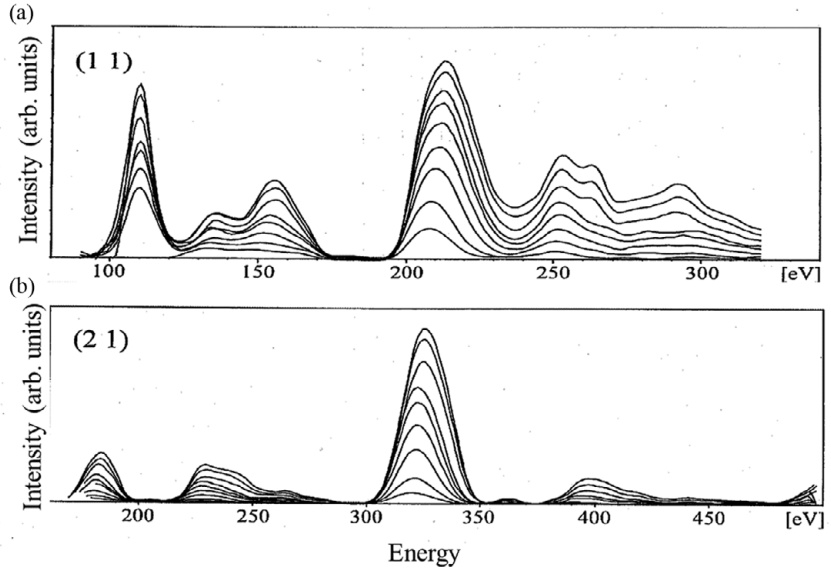

Figure 3.13 Experimental I(V) curves for two diffracted beams (upper and lower panels, respectively) from Cu(110) at various temperatures increasing from 110 K (highest curves) to 465 K (lowest curves). Reprinted from [3.21] W. Moritz, J. Landskron and M. Deschauer, *Surf. Sci.*, vol. 603, pp. 1306–1314, 2009, with permission from Elsevier.

https://doi.org/10.1017/9781108284578.005 Published online by Cambridge University Press

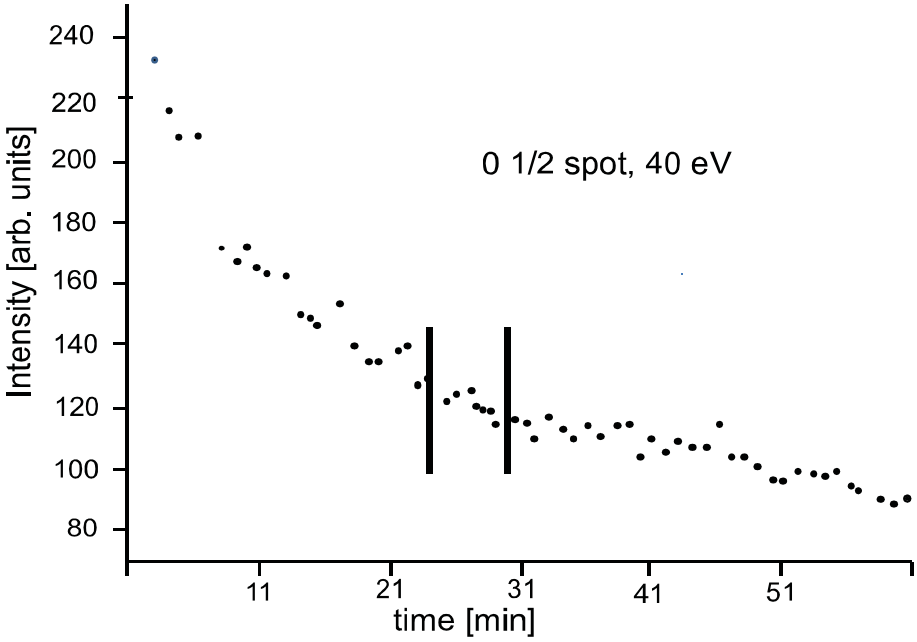

Figure 3.14 Intensity decay due to electron beam damage for thiouracil on Ag(111). The two vertical bars indicate the period chosen for the measurement. Reprinted from [3.21] W. Moritz, J. Landskron and M. Deschauer, *Surf. Sci.*, vol. 603, pp. 1306–1314, 2009. With permission from Elsevier.

The sample should be cooled to liquid nitrogen temperature or lower if possible, because LEED intensities are considerably weakened by thermal vibrations, especially at higher energies. As shown in Figure 3.13, the intensity decreases drastically with increasing temperature (while the background increases, not shown). The measurement at low temperatures exhibits more details in the I(V) curves and less uncertainty due to background subtraction. Also, even more importantly, the calculation of LEED intensities involves rough approximations for vibration amplitudes so that calculated intensities show worse agreement with experiment and higher error bars at higher temperatures.

A check should always be performed by repeating the measurement and evaluating the reproducibility. The sample alignment usually takes much more time than performing the measurement directly after preparation. Therefore, the sample should be prepared afresh and adjusted to the previously determined sample position such that the measurement can be started quickly. Figure 3.14 shows the intensity decay of a superlattice spot of a thiouracil monolayer on Ag(111) due to electron beam damage. The measurements were made after the initial rapid decay, so that during the time of the measurement only a relatively small intensity loss occurred [3.22].

https://doi.org/10.1017/9781108284578.005 Published online by Cambridge University Press

The current in the diffracted beam is usually on the order of a fraction 10^{-2} to 10^{-4} of the primary beam and can be measured with a video camera or directly with a microchannel plate. Modern video techniques allow the measurement of a complete set of I(V) curves in less than 5 minutes.

3.4 Instrumental Response Function

The diffraction spots in the LEED pattern are broadened by two effects: imperfections in the surface and the instrumental response function; the latter concept was introduced by R. L. Park et al. [3.23] to describe the resolution of the LEED instrument. The instrumental response function has several contributions, among which are the energy spread and the angular width of the primary beam, as well as the finite resolution of the detector or fluorescent screen. The convolution of these different contributions leads to an instrumental broadening of the LEED beams which limits the range of defect distributions that can be detected by a beam profile analysis [3.24–3.26].

The instrumental response function represents the beam profile which would be measured from an infinite perfect crystal. The measured angular beam profile may be denoted by $J(\mathbf{q})$, where $\mathbf{q} = \mathbf{k}' - \mathbf{k}$ is the scattering vector. It is given as the convolution of two parts, the beam profile due to imperfections of the surface, $I(\mathbf{q})$, and the instrumental broadening $T(\mathbf{q})$:

$$J(\mathbf{q}) = T(\mathbf{q}) \otimes I(\mathbf{q}) \equiv \int T(\mathbf{q}')I(\mathbf{q}' - \mathbf{q})d\mathbf{q}'. \tag{3.12}$$

The Fourier transform of a convolution is given by the product of the Fourier transforms of the single components and therefore

$$\mathrm{F}\{J(\mathbf{q})\} = \mathrm{F}\{T(\mathbf{q})\}\mathrm{F}\{I(\mathbf{q})\} = t(\mathbf{u})P(\mathbf{u}). \tag{3.13}$$

The quantity $t(\mathbf{u}) = \mathrm{F}\{T(\mathbf{q})\}$ is defined as the transfer function. The full width at half maximum (FWHM) is defined as the transfer width [3.23]. The Fourier transform of the diffracted intensity $I(\mathbf{q})$ is the Patterson function $P(\mathbf{u})$, that is, the autocorrelation function of the crystal structure; $\mathbf{u}$ is the distance vector between two scatterers. The autocorrelation function $P(\mathbf{u})$ is a measure of the number of pairs of scatterers that are separated by a vector $\mathbf{u}$. It is a vector in real space; we use the symbol $\mathbf{u}$ to distinguish the distance vector from a position vector $\mathbf{r}$ of the atoms. From $P(\mathbf{u})$, information can be derived about the periodic structure and, in the case of disordered surfaces, about the defect distribution. In principle, $P(\mathbf{u})$ could be determined if $T(\mathbf{q})$ and $J(\mathbf{q})$ could be measured accurately. However, in practice, both $T(\mathbf{q})$ and $J(\mathbf{q})$ have uncertainties associated with them and the function $I(\mathbf{q})$ cannot be determined with a width less than the sum of the uncertainties in the widths of $T(\mathbf{q})$ and $J(\mathbf{q})$.

Equation (3.13) implies that the correlation between two scatterers cannot be detected in the range in which $t(\mathbf{u})$ is zero, normally for larger distances. Hence, the transfer width is regarded as the effective coherence length of the instrument.

https://doi.org/10.1017/9781108284578.005 Published online by Cambridge University Press

However, it does not represent a limit on the region over which phase correlation exists or can be detected, as has been discussed by G. Comsa [3.27].

The angular divergence of the primary beam of most of the commercially available LEED systems is about 0.5°, together with a limited energy resolution of 0.1–0.2 eV. The transfer width determined by measuring the angular profile of a diffracted beam varies typically between 2 and 10 nm. This resolution is sufficient for structure analysis but is poor for the analysis of defect distributions. Therefore, the observation of an apparently 'good' LEED pattern in a conventional LEED system with sharp spots and low background does not guarantee a low concentration of defects or a surface free of contaminants. For the analysis of defect distributions, high-resolution LEED systems have been developed with a transfer width of up to 400 nm [3.4; 3.28; 3.29], as discussed in Section 3.6.1.

3.5 Brief Overview of Types of Available LEED Systems

LEED systems are commercially available, leading to their widespread use in surface science. A number of systems are offered by different companies; we describe only some types here. It is not our intention to review all available systems, nor to make recommendations.

There are mainly three different types of systems on offer. Widely used are display systems with a fluorescent screen; for example, Figure 3.15 shows a system from SPECS, which is also equipped with a shutter for protection of the screen. The system is based on a design developed by P. Heilmann et al. [3.3] in the group of K. Heinz and K. Müller, who also pioneered the development of video measurements of LEED intensities.

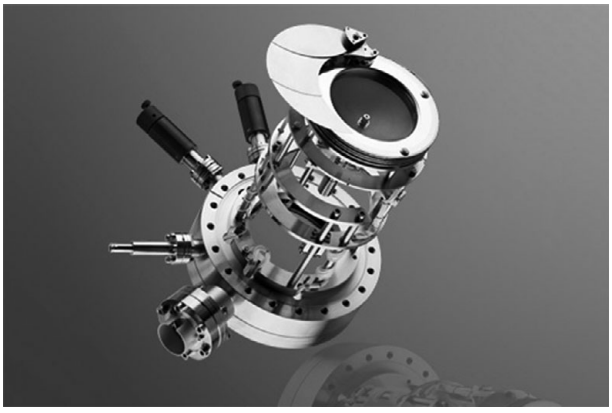

Figure 3.15 LEED system with a phosphorescent screen, ErLEED 100/150, Reverse View LEED SPECS. Reprinted from [3.30] www.specs.de, with permission from SPECS GmbH, Berlin, Germany.

https://doi.org/10.1017/9781108284578.005 Published online by Cambridge University Press

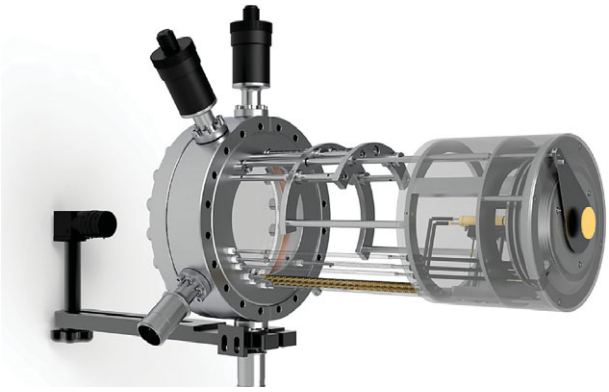

Figure 3.16 Microchannel plate system (MCP-LEED), LEED 800 MCP, LEED for Organic Films & Molecular Beam Epitaxy (Scienta Omicron, Uppsala, Sweden and Taunusstein, Germany). Reprinted from [3.31] www.scientaomicron.direct/96/electron-diffraction/femto, with permission.

The primary beam current used with the fluorescent screen is usually on the order of 100 nA, which corresponds to about 0.1 electron per surface atom per second. Materials which are sensitive to electrons and insulating surfaces require lower currents. For this purpose, a microchannel plate (MCP) for intensifying the diffracted beams can be used in front of a fluorescent screen. The primary current can be as low as 5 nA with a single microchannel plate and down to 100 pA with a double microchannel plate. The LEED pattern can then be viewed on a fluorescent screen behind the microchannel plate(s). The aberrations in the LEED pattern caused by the use of a planar screen and microchannel plates can be eliminated by correction field plates. An example of a microchannel plate system from Scienta Omicron is shown in Figure 3.16 [3.31].

A fluorescent screen is usually combined with a CCD camera to measure the LEED intensities from the image on the screen. To obtain high quality LEED I(V) data a highly-sensitive 12-bit digital camera is required. However, this is not necessary when a position sensitive detector is used behind the microchannel plate. The direct measurement with a delay line detector allows an even lower current down to the fA range, so the digital image can be directly stored and no camera is needed. The low current allows a small focus of the primary beam and the investigation of insulating surfaces. A model from OCI Vacuum Microengineering is shown in Figure 3.17 [3.32].

The use of microchannel plates and position sensitive detectors has the disadvantage that these components are usually sensitive to venting the UHV system, due to contamination by air, which is not the case for the fluorescent screen.

Systems have also been developed for special applications, for example a LEED system combined with evaporation sources to observe in situ the structures formed during adsorption; this capability is mainly applied to the study of organic molecules [3.33].

https://doi.org/10.1017/9781108284578.005 Published online by Cambridge University Press

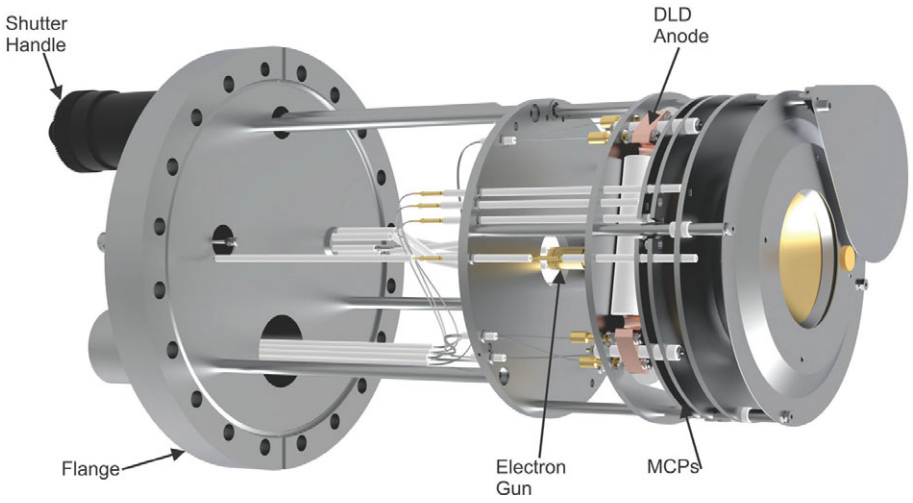

Figure 3.17 FemtoLEED spectrometer DLD-L800 with integral shutter (OCI Vacuum Microengineering). Reprinted from www.ocivm.com, with permission from OCI Vacuum Microengineering, Inc.

3.6 High-Resolution Instruments

As mentioned in Section 3.4, the transfer width of most LEED systems is in the range of about 2–10 nm. This means that such systems cannot detect spatial correlations between scatterers spaced farther apart than about 2–10 nm; thus, spatial ordering (in particular crystallinity, such as domain and island sizes) cannot be resolved over larger distances: this is considered to be low resolution. High-resolution instruments have transfer widths up to 400 nm or even more, corresponding to very narrow reflection profiles, provided the sample is perfect. Instruments producing a direct image of the surface are LEEM (low-energy electron microscope) and PEEM (photoemission electron microscope). We discuss LEEM in Section 3.6.2. With LEEM a resolution of 5 nm can be reached due to substantial improvements of the electron lenses since the first instruments were built. Even higher resolution may be possible in the future. The direct imaging of STM and AFM produces much higher spatial resolution (on the order of many microns) and is not considered here.

3.6.1 Spot Profile Analysis LEED (SPA-LEED)

To study the distribution of surface defects with high resolution requires specially designed electron guns and collimating systems known as high-resolution LEED (HR-LEED) or SPA-LEED. Spot profile analysis was developed by U. Scheithauer

https://doi.org/10.1017/9781108284578.005 Published online by Cambridge University Press

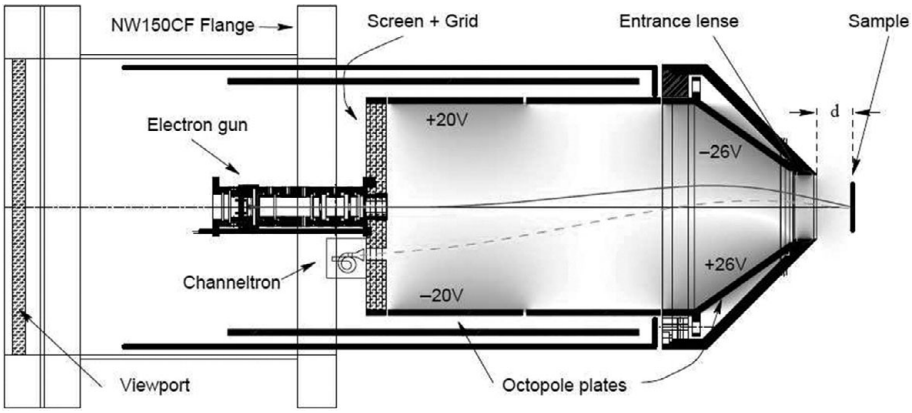

Figure 3.18 Horizontal cut through a third generation SPA-LEED with conical shape. Shown are the electron gun, the channeltron detector, the electrostatic deflection unit, the entrance lens and the sample in a position with distance d. The potential of the electrostatic deflection field is shown in a grey scale representation. The path for the incident electron beam and the path of those electrons which are recorded in the detector are shown. During scanning across the sample, the spot position on the sample stays constant. The scan is done by moving the focus at the detector. Republished with permission of Walter de Gruyter and Company, from [3.34] M. Horn-von Hoegen, *Z. Krist.*, vol. 214, pp. 591–629, 1999; permission conveyed through Copyright Clearance Center, Inc.

et al. [3.4] in the group of M. Henzler. The SPA-LEED instrument is a high-resolution LEED system with an octopole lens to collimate the primary and diffracted beams. The instrument and applications have been described in detail by M. Horn-von Hoegen [3.34]. The instrument has an internal electron gun, but an external gun can be applied to allow in-situ observation of growth processes. Commercially available is a system which reaches a transfer width of up to 400 nm. The dynamic range is 100-times higher than in conventional LEED systems. A schematic drawing of a cut through the instrument is shown in Figure 3.18 and a view of the new commercially available system is shown in Figure 3.19. Scienta-Omicron no longer produces the SPA-LEED system; however, a newly-designed system and new software are available from a new company [3.35].

The diffracted intensities are measured with a channeltron and the diffraction pattern is electronically stored. The spot profiles can be evaluated. An example of the diffraction pattern for the Si(111)-(7×7) reconstruction is shown in Figure 3.20, demonstrating the high resolution.

The diffraction intensities measured with the channeltron are not suited for I(V) analysis since the incidence angle is not constant but different for each spot. Some I(V) measurements are possible, nevertheless. The instrument has a phosphorescent screen, on which the diffracted intensities can be observed and measured with a video camera keeping the incidence angle constant; see Figure 3.21. The aperture of the

https://doi.org/10.1017/9781108284578.005 Published online by Cambridge University Press

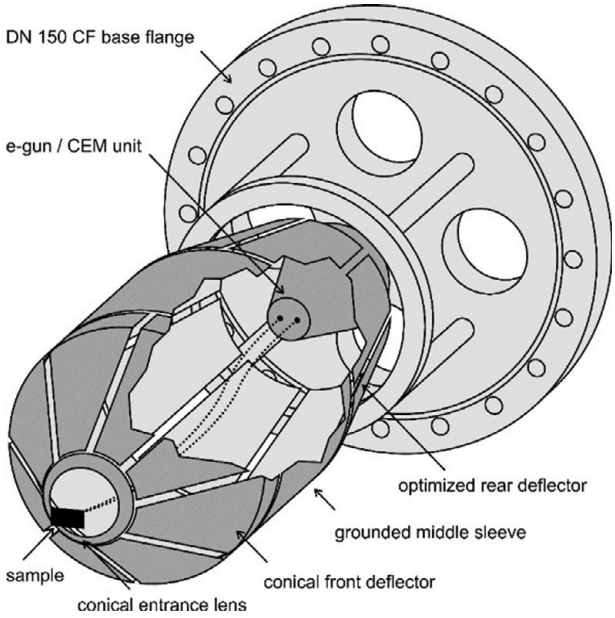

Figure 3.19 View of the new SPA-LEED system mounted on an 8″ flange. The fourth generation of the SPA-LEED system shows a highly symmetric design with round octopole deflectors and a compact and centred e-gun/CEM unit in order to minimise the image distortions and to increase the angular scan range. With permission from [3.35] Dr. Peter Kury, out-of-the-box systems GmbH.

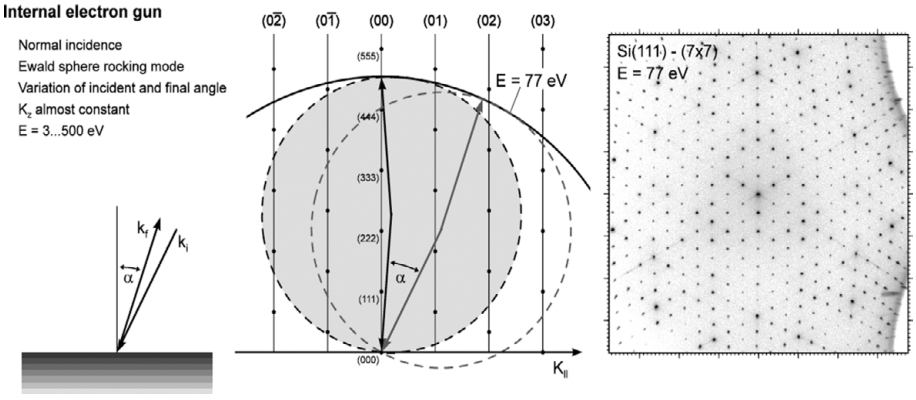

Figure 3.20 Diffraction geometry in reciprocal space for the SPA-LEED internal electron gun. The angles of the incident electron beam and of the diffraction pattern are both varied continuously in order to record the LEED pattern. The relative angle between incident and final scattering vectors stays constant. As a result, the recorded diffraction pattern is described by the envelope of the rocking Ewald sphere, that is, a sphere centred at the origin of the reciprocal space with a diameter twice the size of the Ewald sphere. The high-resolution pattern shown on the right is for Si(111)-(7×7) at 77 eV. Typical electron energies are 30–120 eV. Republished with permission of Walter de Gruyter and Company, from [3.34] M. Horn-von Hoegen, *Z. Krist.*, vol. 214, pp. 591–629, 1999; permission conveyed through Copyright Clearance Center, Inc.

https://doi.org/10.1017/9781108284578.005 Published online by Cambridge University Press

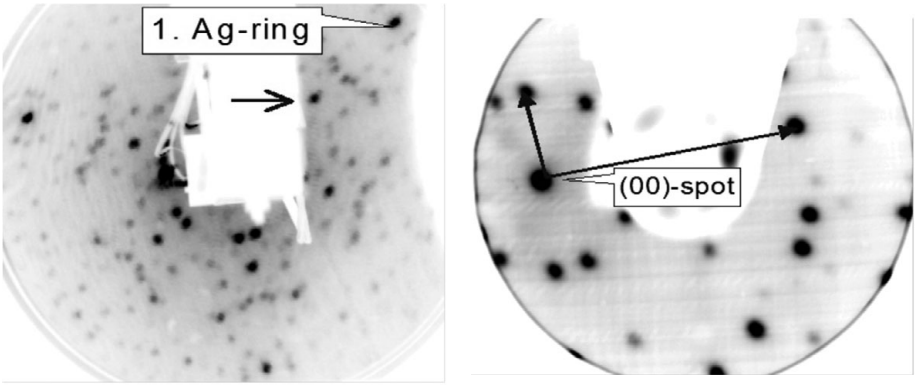

Figure 3.21 Diffraction patterns from thiouracil/Ag(111) from different LEED systems. Left panel: conventional LEED system; right panel: SPA-LEED system. Both images are taken from the same sample at 50 eV and 147 K. In the right panel, most of the first ring of 12 superlattice spots around the specular beam is visible on the left; in the left panel the specular beam and this ring are obscured by the specimen holder (bright object). The corresponding rings around three substrate reflections appear weakly in the left panel. The arrow marks the (0,1/2) spot. Reprinted from [3.21] W. Moritz, J. Landskron and M. Deschauer, *Surf. Sci.*, vol. 603, pp. 1306–1314, 2009. With permission from Elsevier.

screen is not as large as with conventional systems, but the high collimation of the primary beam allows measurements which cannot be resolved by a conventional LEED system.

3.6.2 Low-Energy Electron Microscopy (LEEM)

High resolution is also achieved by low-energy electron microscopy (LEEM), which allows the observation of the direct image as well as measurement of diffracted intensities; see Figure 3.22. The instrument was developed by W. Telieps and E. Bauer [3.5] in 1985. Several instruments have been built and are commercially available (see the link within [3.5] for further references and information about the capabilities of the LEEM instrument and its applications). The resolution achieved with LEEM can be as low as about 5 nm and allows the measurement of diffraction intensities from small areas and single domains, which is usually not possible with conventional LEED systems. Dark field images using the superlattice beams show the individual domains; an example is given in Figure 3.23 for Si(100) where the two domains with (2×1) and (1×2) reconstruction in different terraces are made visible.

The specular beam at normal incidence can be measured by the deflection of the primary and diffracted beam through the beam splitter. A further advantage is the fixed spot position on the screen with varying energy. Instruments equipped with additional experimental facilities are: SPELEEM (spectroscopic measurements),

https://doi.org/10.1017/9781108284578.005 Published online by Cambridge University Press

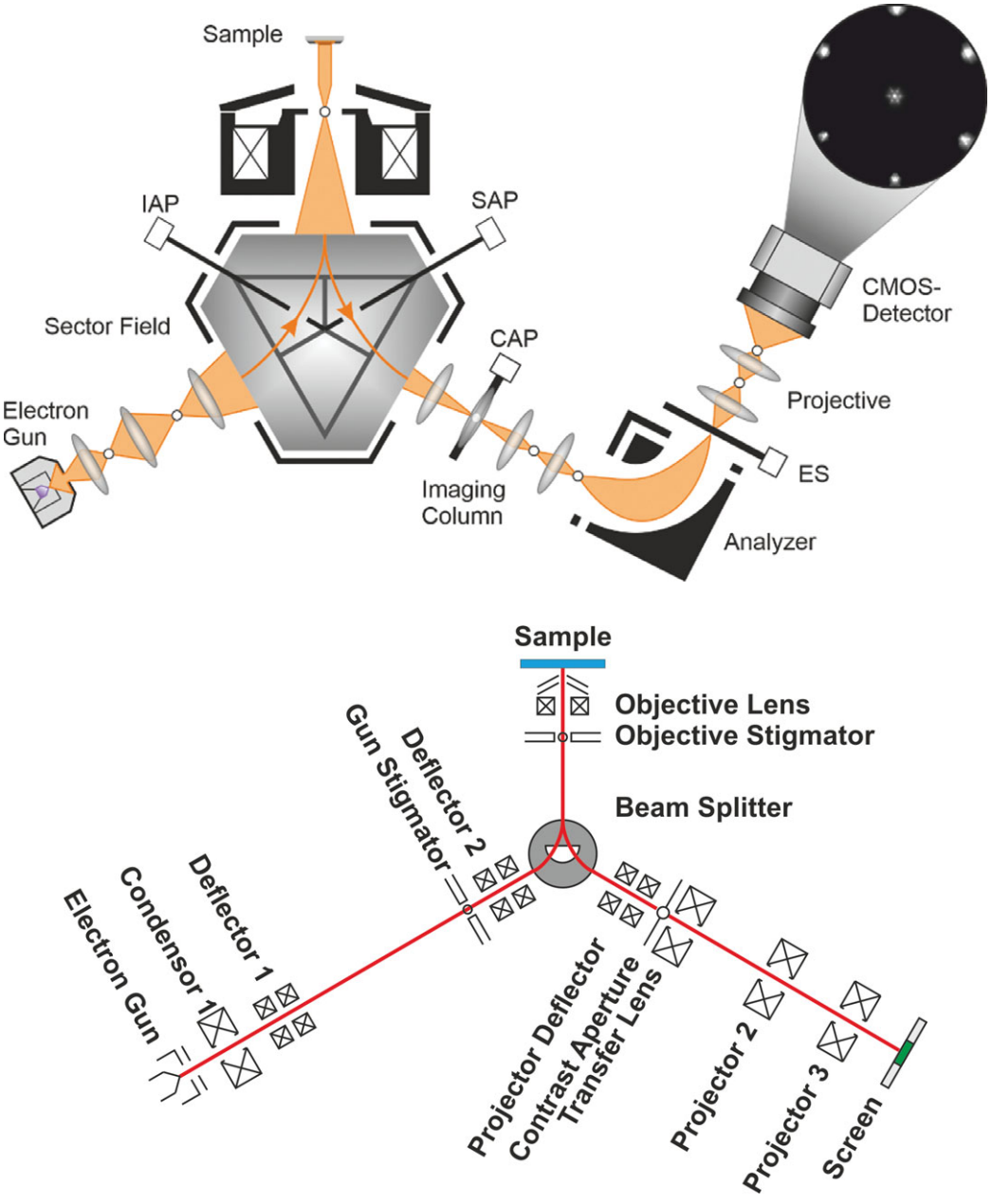

Figure 3.22 Schematic drawings of two LEEM instruments. The upper panel shows the beam path with an energy analyser in the diffracted beam. The diffraction pattern is from the reconstructed Au(111) surface and shows the satellite reflections around the (00) spot. Courtesy of F.-J. Meyer zu Heringsdorf, University Duisburg-Essen, with permission.

https://doi.org/10.1017/9781108284578.005 Published online by Cambridge University Press

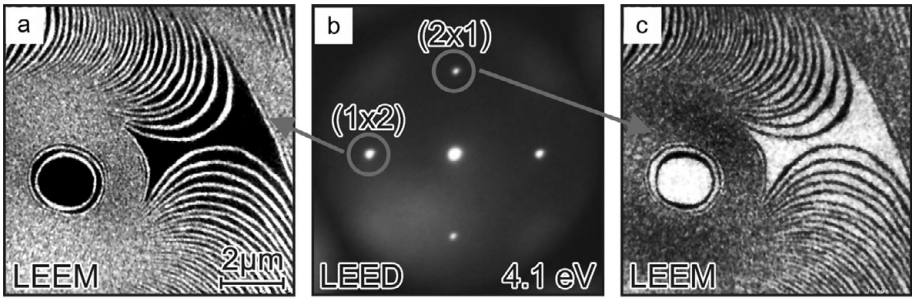

Figure 3.23 Dark field LEEM images from (2×1) and (1×2) domains of Si(100). The diffraction pattern shows the (00) spot and the (0, ±1/2) and (±1/2, 0) spots of the two domains: the selected spot highlights its corresponding domain orientation. Reproduced with permission from [3.36] P. Kirschbaum, L. Brendel, K. R. Roos, M. Horn-von Hoegen and F.-J. Meyer zu Heringdorf, *Mater. Res. Express*, vol. 3, p. 085011, 2016 (Open Access).

SPLEEM (spin polarised), and instruments that allow both spectroscopic and spin resolved measurements.[1]

3.7 Some Developments for Special Applications

3.7.1 In-situ Observation of Adsorption Processes

Some conventional LEED instruments have been modified in the past two decades for special applications and improved measurement methods. A system allowing the study of sensitive surface structures with low electron doses using a slow scan CCD camera has been developed by G. Held et al. [3.37]. The observation of the diffraction pattern during deposition of adsorbates can be used to study phase transformations and phase transitions. An arrangement which allows real time monitoring of phase transitions of vacuum deposited organic films has been described by C. Seidel et al. [3.33]. Frequently, there is a need to prepare surfaces and monitor them by LEED, prior to further investigation in a different chamber without breaking the vacuum; this is achieved by a transport chamber for interconnection with other experiments [3.38].

3.7.2 Nanostructures

A compact UHV system has been developed in order to fabricate and analyse micro- and nanostructures on surfaces in situ [3.39]. The observation of nanostructures by LEED requires a LEED beam with a very small focus. The diameter of the primary beam usually depends on energy and beam intensity. It is difficult to focus a

[1] For commercially available instruments see: https://elmitec.de and www.specs-group.com/nc/specsgroup/knowledge/applications/productlines/detail/leempeem/, 2021.

https://doi.org/10.1017/9781108284578.005 Published online by Cambridge University Press

low-energy electron beam because of the space charge effect which broadens the beam. The width usually varies from about 500 μm at low energies to 100 μm at higher energies and depends on the design of the electron gun. The system reported by Y. Kakefuda et al. [3.39] includes a low-energy electron gun which provides a minimum spot size of about 25 nm using electrostatic lenses, AES, EELS and a LEED optic.

3.7.3 Convergent Beam LEED

The transfer width of a conventional LEED system can be substantially improved from 10 nm to about 70 nm by a modulated beam combined with a time resolved collection of LEED images [3.40]. A convergent beam LEED (CBLEED) technique has been proposed [3.41] in analogy to the related technique in X-ray diffraction. The diffraction disks, replacing sharp spots, show the angular dependence of the diffraction intensity. The use of an STM tip as electron source could produce LEED patterns from areas as small as 50 nm.

3.7.4 Ultrafast Measurements

Recently RHEED has been used in combination with a pulsed photocathode to study the dynamics of ultrafast processes at surfaces [3.42]. The surface is excited by

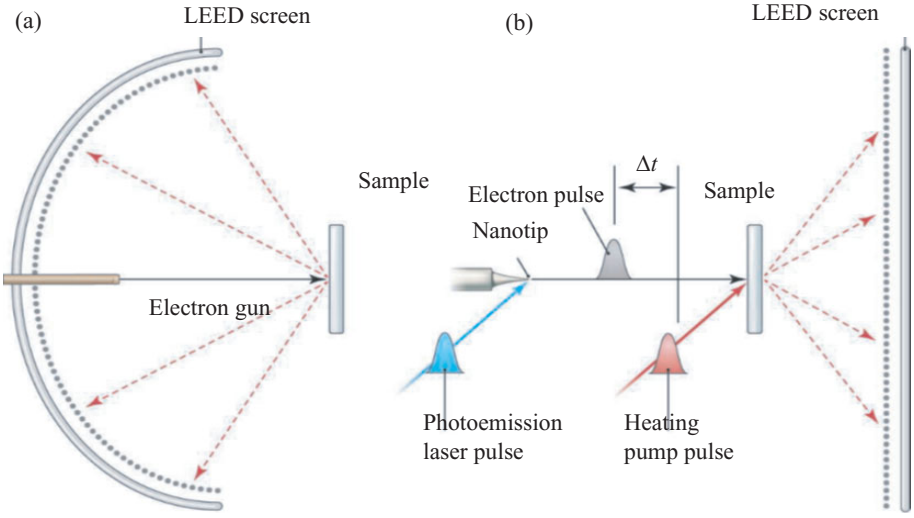

Figure 3.24 (a) Conventional LEED works by reflecting electrons back to a phosphor screen. (b) Transmission ultrafast LEED (T-ULEED). From [3.47] E. T. J. Nibbering, *Science*, vol. 345, pp. 137–138, 2014, https://doi.org/10.1126/science.1256199. Reprinted with permission from AAAS (online readers may view, browse and/or download material for temporary copying purposes only, provided these uses are for noncommercial personal purposes. Except as provided by law, this material may not be further reproduced, distributed, transmitted, modified, adapted, performed, displayed, published or sold in whole or in part, without prior written permission from the publisher).

femtosecond laser pulses and the transient changes of surface structure (e.g., upon excitation of a phase transition) is followed in a stroboscopic pump probe scheme [3.43; 3.44]. A temporal resolution of less than 330 fs has been achieved with a pulsed electron gun at high energies [3.45]. M. Gulde et al. [3.46] achieved time resolution in the picosecond regime with a pump-probe configuration in their transmission ultrafast LEED (T-ULEED) experiment with electron pulses lasting a few picoseconds; see Figure 3.24(b). Transmission electron diffraction patterns were obtained from bilayer graphene covered with PMMA (polymethylmethacrylate) at an electron energy of 1 keV [3.47].

The electron pulses are generated from a sharp tungsten tip (50 nm radius of curvature) by illumination with a second-harmonic pulse originating from the same laser output as the laser pump pulse [3.48]. This method ensures accurate time delay between the two pulses.

https://doi.org/10.1017/9781108284578.005 Published online by Cambridge University Press